PCCP

ROYAL SOCIETY OF CHEMISTRY

PAPER

View Article Online
View Journal | View Issue

Check for updates

Cite this: *Phys. Chem. Chem. Phys.*, 2023, **25**, 2043

Electronic state evolution of oxygen-doped monolayer WSe_2 assisted by femtosecond laser irradiation†

Lei Wang, ‡[a] Dan Wang,‡[b] Yang Luo,‡[ac] Chen-Yu Xu,[a] Lin Cui,[a] Xian-Bin Li [a] and Hong-Bo Sun *[d]

Received 27th September 2022,
Accepted 29th October 2022

DOI: 10.1039/d2cp04495a

rsc.li/pccp

Electronic states are significantly correlated with chemical compositions, and the information related to these factors is especially crucial for the manipulation of the properties of matter. However, this key information is usually verified by after-validation methods, which could not be obtained during material processing, for example, in the field of femtosecond laser direct writing inside materials. Here, critical evolution stages of electronic states for monolayer tungsten diselenide (WSe_2) around the modification threshold (at a Mott density of $\sim 10^{13}$ cm^{-2}) are observed by broadband femtosecond transient absorption spectroscopy, which is associated with the intense femtosecond-laser-assisted oxygen-doping mechanism. First-principles calculations and control experiments on graphene-covered monolayer WSe_2 further confirm this modification mechanism. Our findings reveal a photochemical reaction for monolayer WSe_2 under the Mott density condition and provide an electronic state criterion to *in situ* monitor the degrees of modification in monolayer transition metal dichalcogenides during the femtosecond laser modification.

Introduction

In recent years, 2D materials like transition metal dichalcogenides (TMDCs) have been intensively studied for the next-generation nano-optoelectronic devices,[1–5] due to their flexibility and atomic thickness,[6,7] along with their excellent electrical and mechanical properties.[8] To manipulate the properties of 2D materials, defect/doping engineering is proposed,[9] which could endow pristine 2D materials with novel functions. For example, photon/electron/neutron beams have been used to dope 2D materials by changing chemical compositions, in which lateral transistor and photodetector structures are achieved.[10–13] On the other hand, laser direct writing and patterning under intense irradiation conditions have been introduced to create 2D micro–nanostructures by removing undesired parts of 2D materials or induce changes of chemical compositions in the irradiation part, where unique optoelectronic responses in ultrathin flat lenses, logic circuits and synaptic devices are reported.[14–16]

Although these doped 2D materials are well characterized by Raman spectroscopy and X-ray photoelectron spectroscopy (XPS) after material processing, which demonstrates the resulting composition changes, the key defect physics during the electronic state evolution of pristine samples is missing. In particular, when ultra-short laser pulses with a high energy density are closely focused on the surface of 2D TMDCs, a series of initial physical and chemical processes like the lattice distortion and the following generation of defect states would occur, which are the beginning of irreversibly changing physical and chemical properties of TMDCs in the fabrication/modification threshold.[17–21] Therefore, more accurately finding this threshold requires a deeper understanding of the initial defect/doping physics under intense laser irradiation on TMDCs. Aiming at this 'black box' between the initial state before laser modification and the final state after laser modification, it is urgent to develop an *in situ* detection technology to indicate the electronic state evolution during femtosecond laser irradiation on the surface of TMDCs.

In this paper, we present crucial evolution stages of electronic states for monolayer WSe_2 under intense femtosecond laser irradiation (IFsLI) by broadband femtosecond transient absorption

[a] *State Key Laboratory of Integrated Optoelectronics, College of Electronic Science and Engineering, Jilin University, 2699 Qianjin Street, Changchun 130012, China*
[b] *Department of Mechanical Engineering and Materials Science, Yale University, New Haven, CT 06511, USA*
[c] *Changchun Institute of Optics, Fine Mechanics and Physics, Chinese Academy of Sciences, Changchun 130033, China*
[d] *State Key Laboratory of Precision Measurement Technology and Instruments, Department of Precision Instrument, Tsinghua University, Haidian, Beijing 100084, China. E-mail: hbsun@tsinghua.edu.cn*

† Electronic supplementary information (ESI) available. See DOI: https://doi.org/10.1039/d2cp04495a

‡ Lei Wang, Dan Wang and Yang Luo contributed equally to this work.

(TA) spectroscopy. With the help of precise control of the sample position by a 3D motion stage, we demonstrate the transient influence of femtosecond-laser-assisted oxygen atom doping on the electronic structure of monolayer WSe_2. First-principles calculations[22–24] and control experiments on graphene-covered monolayer WSe_2 are also performed to support this modification mechanism. Different from previous reports on laser fabrication in 2D WSe_2,[14–16] which particularly emphasize the resulting functionality of prepared devices, our findings provide a solution to directly observe electronic state evolution around the modification threshold of monolayer WSe_2 and *in situ* monitor the degrees of modification in monolayer transition metal dichalcogenides during the femtosecond laser modification.

Experimental

Sample preparation

CVD grown monolayer WSe_2 continuous films and graphene-covered monolayer WSe_2 films were purchased from Sixcarbon technology, Shenzhen, China. These monolayer films were prepared by the CVD method on SiO_2/Si substrates and then transferred to sapphire or quartz substrates. For graphene-covered monolayer WSe_2 films, the graphene was first coated with a layer of polymethyl methacrylate (PMMA), and then the PMMA-support graphene film was transferred onto the monolayer WSe_2 continuous film on quartz substrates. The prepared graphene-covered monolayer WSe_2 was immersed in acetone to remove the outside PMMA on the surface of the graphene, and then it was vacuum annealed at 300 °C for 2 hours.

Steady-state characterizations

The steady-state absorption spectra were measured using a home-built micro-zone optical microscope system. The Raman and steady-state PL spectra were measured using Alpha 300R (532 nm excitation). X-ray diffraction (XRD) data were recorded on a Rigaku D/Max-2550 diffractometer with CuKα radiation (λ = 0.15418 nm).

Femtosecond broadband TA system

We used a mode-locked Ti:sapphire amplifier to generate 800 nm (repetition rate: 500 Hz) laser pulses with 35 fs pulse width (Solstice, Spectra-Physics). It was split into two beams: one was used as pump lights (400 nm pump lights); the other was through a cuvette of 2 mm water, producing a broadband probe light (ranging from 400 nm to 850 nm).[25–27] The signals of TA were collected using a fiber-coupled spectrometer. The dispersion correction of TA data was performed by a chirp program. All TA experiments are performed at room temperature. The samples were fixed on an electrically controlled 3D motion stage so that the fresh area on the sample was measured for each laser shot when the pump power was larger than the estimated modification threshold. Namely, for relatively high pump powers (initial exciton densities were estimated from 6.82×10^{12} to 1.89×10^{13} cm^{-2}), only a single TA spectrum of fresh monolayer WSe_2 was recorded at a given delay time. It avoided the influence of long exposure time on TA data under high pump power conditions. When each TA experiment is finished at a given pump density, the pump light is blocked by a mechanical shutter, and the sample is checked out back-to-back using the nearby optical microscope system. Thus, we can assign pump densities to optical images of femtosecond laser modified monolayer WSe_2.

Theoretical calculations

We performed the calculations using density functional theory (DFT)[28–31] as implemented in the VASP codes.[32,33] The exchange-correlation energy was described by the generalized gradient approximation, in the scheme proposed by Perdew, Burke and Ernzerhof (PBE).[34] A $6 \times 6 \times 1$ supercell of WSe_2 is used in the calculations. The cell size in the *z*-direction is 15 Å for the perfect and doped systems. The cutoff energy for the plane wave basis is 520 eV and a $3 \times 3 \times 1$ Monkhorst–Pack mesh grid is used for *k*-point sampling. All atoms were relaxed until the Hellman–Feynman forces on individual atoms were less than 0.02 eV $Å^{-1}$. During the calculations of defect formation energy, the chemical potential of W and Se under W-rich and S-rich conditions are referred to as W (bcc) and Se (trigonal phase) crystals, respectively. We have referred to the chemical potential of the O atom to its reservoir O_2 and WO_3 (*P6mmm*).

Results and discussion

Fig. 1a shows the steady-state absorption spectra of monolayer WSe_2 on the sapphire substrate with/without IFsLI treatments (pumped at 400) measured using a home-built micro-zone optical microscope system. For pristine monolayer WSe_2, there are four exciton states, labelled as A-exciton, B-exciton, A′-exciton, and C-exciton states, respectively. A-exciton and B-exciton states are the band-edge states due to the spin–orbital splitting at the *K* point, A′-exciton state is related to the high-energy excited-state levels of the A-exciton state, and the C-exciton state is originated from the band-nesting region in the band structure.[35–38] For the IFsLI treatment, the IFsLI case 1 represents a moderate modification for monolayer WSe_2. And the IFsLI case 2 represents a strongly modified result for monolayer WSe_2. As a result, the B-exciton and A′-exciton states of monolayer WSe_2 almost disappeared in the steady-state absorption spectrum of IFsLI case 2. Typical micro-zone optical images for IFsLI case 1 and IFsLI case 2 are shown in Fig. S1 (ESI†). Fig. 1b presents the Raman spectra of pristine monolayer WSe_2 and IFsLI-treated monolayer WSe_2. It indicates a gradually redshift trend for the Raman peak of degenerated E^1_{2g} and A_{1g} modes from 250.7 cm^{-1} in pristine monolayer WSe_2 to 247.0 cm^{-1} in IFsLI case 2. This softening of Raman modes implies n-type doping for IFsLI-treated monolayer WSe_2.[39,40] Fig. 1c shows the steady-state photoluminescence (PL) spectra of pristine monolayer WSe_2 and IFsLI-treated monolayer WSe_2, which indicate a decreased trend for the radiation recombination intensities. The PL peak fitting analyses for the three

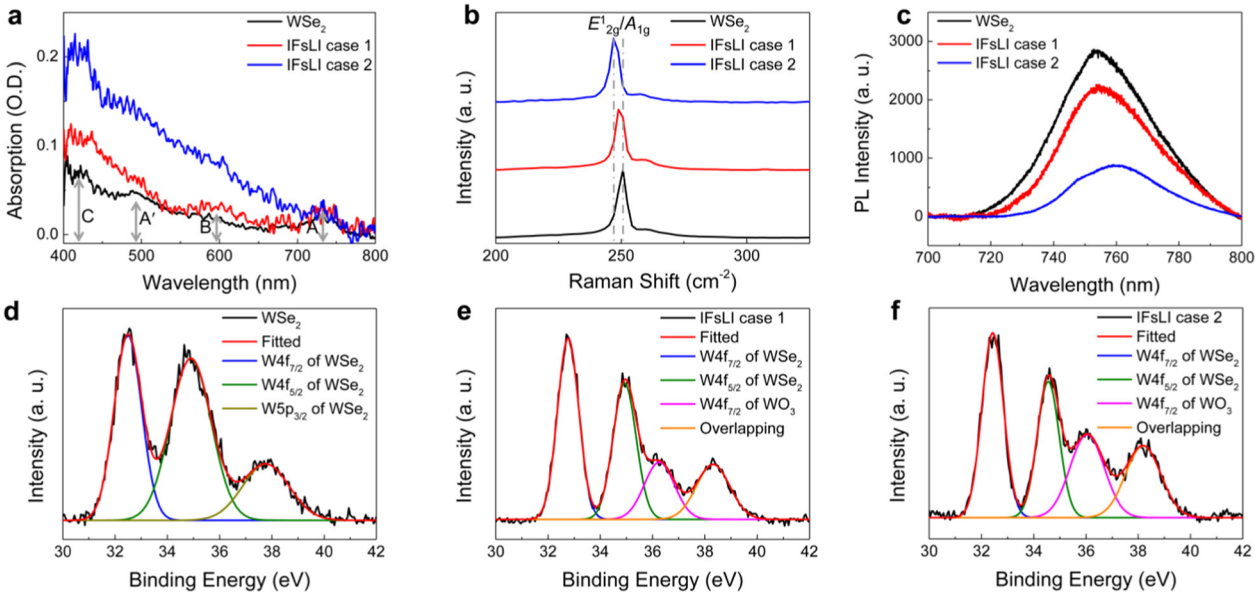

Fig. 1 (a) Steady-state absorption spectra, (b) Raman spectra, and (c) steady-state PL spectra of pristine monolayer WSe_2 on the sapphire substrate and IFsLI-treated monolayer WSe_2. XPS analysis for (d) pristine monolayer WSe_2 on the sapphire substrate, (e) monolayer WSe_2 with a moderate modification (IFsLI case 1), and (f) monolayer WSe_2 with a strong modification (IFsLI case 2).

samples are presented in Fig. S2 (ESI†). It suggests that the contribution of defects to the PL spectrum is gradually increased, which is ~8% in pristine monolayer WSe_2, ~18% in IFsLI case 1, and ~49% in IFsLI case 2 (Table S1, ESI†).

The XPS measurements further confirm the origin of IFsLI-related doping for monolayer WSe_2. For pristine monolayer WSe_2 (Fig. 1d), there are three XPS peaks at 32.49 eV, 34.90 eV, and 37.77 eV, corresponding to the binding energy of $W4f_{7/2}$ (WSe_2), $W4f_{5/2}$ (WSe_2), and $W5p_{3/2}$ (WSe_2), respectively.[41,42] For IFsLI case 1 (Fig. 1e), the XPS peaks of $W4f_{7/2}$ (WSe_2) and $W4f_{5/2}$ (WSe_2) are at 32.77 eV and 34.93 eV, respectively. More importantly, there is an additional XPS peak at 36.36 eV for the binding energy of $W4f_{7/2}$ (WO_x) in the XPS spectrum of IFsLI case 1. It implies there is an overlapping state for the XPS peak at 38.32 eV, in which XPS peaks of $W5p_{3/2}$ (WSe_2) and $W4f_{5/2}$ (WO_x) could be mixed together.[14,15] For IFsLI case 2 (Fig. 1f), the XPS peaks of $W4f_{7/2}$ (WSe_2) and $W4f_{5/2}$ (WSe_2) are at 32.43 eV and 34.44 eV, respectively. Moreover, the ratio of the XPS peak at 36.04 eV for the binding energy of $W4f_{7/2}$ (WO_x) in IFsLI case 2 becomes larger. All the parameters for the fitting of W-related XPS peaks are listed in Table S2 (ESI†). Based on the XPS data, we could estimate that the amount of oxide is ~29% and ~40% for IFsLI cases 1 and 2, respectively. So, XPS and Raman measurements indicate the formation of new oxygen-related defects is responsible for n-doped monolayer WSe_2 under the IFsLI treatment under our experimental conditions. We prefer to adopt WO_3 denoted as the main oxygen-related defect state, according to the following TA spectra of IFsLI-treated monolayer WSe_2.

To reveal the modification processes in IFsLI-treated monolayer WSe_2, broadband femtosecond TA experiments from low pump densities to high pump densities are performed. Fig. 2 shows initial TA spectra for monolayer WSe_2 under 400 nm excitation. Under 400 nm excitation conditions, we can estimate the initial exciton density of monolayer WSe_2, based on the absorption value of pristine monolayer WSe_2 at 400 nm.

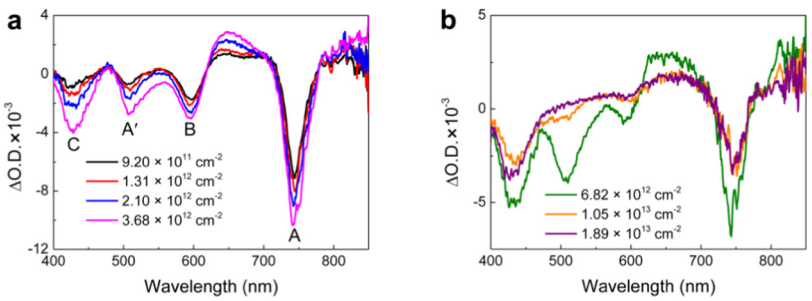

Fig. 2 (a) Initial TA spectra of monolayer WSe_2 probed at 0.36 ps under 400 nm at relatively low initial exciton densities from 9.20×10^{11} cm^{-2} to 3.68×10^{12} cm^{-2}. (b) Initial TA spectra of monolayer WSe_2 probed at a given delay time (*i.e.*, ~1 ps) under 400 nm at relatively high initial exciton densities from 6.82×10^{12} to 1.89×10^{13} cm^{-2}, where the initial exciton density of 6.82×10^{12} cm^{-2}, 1.05×10^{13} cm^{-2}, and 1.89×10^{13} cm^{-2} corresponds to the beginning of IFsLI treatment, the moderate modification conditions (IFsLI case 1), and the strong modification conditions (IFsLI case 2), respectively.

At the relatively low initial exciton densities from 9.20×10^{11} cm^{-2} to 3.68×10^{12} cm^{-2} (Fig. 2a), the peak amplitude and peak broadening of the four ground state bleaching (GSB) signal increase as initial exciton densities. We find these transient features start to become strange (Fig. 2b), when the initial exciton density is further increased from 6.82×10^{12} cm^{-2} (we assign this exciton density as the critical threshold for IFsLI-treated monolayer WSe_2) to a Mott density of $\sim 10^{13}$ cm^{-2}.[43] For the initial exciton density of 6.82×10^{12} cm^{-2}, the initial GSB signals for band-edge A-exciton and B-exciton states are greatly decreased, implying the reduced oscillator strength (due to the increased defects[35]) and/or decreased total amount (due to the cost of oxidizing of WSe_2) for the component of pure WSe_2 in the overlapping area of pump–probe light spots. Besides, in the spectral range from 500 nm to 700 nm, a broad positive signal appears which is usually attributed to new products in TA experiments. The signals corresponding to the B-exciton bleaching state even become positive for IFsLI case 1 and IFsLI case 2 under the Mott density condition, probably due to the spectral overlapping with this broad positive signal. In particular for the stronger modification conditions (IFsLI case 2, an initial exciton density of 1.89×10^{13} cm^{-2}), the initial GSB signal for A′-exciton state disappears, and the initial TA signals in the spectral range of 500–700 nm look like an overlapping of TA signals in monolayer WSe_2 and hole-dominant WO_3 (Fig. S3, ESI†).[44–48] It could be due to the electron transfer from oxidized areas (the defects like WO_3 clusters) to the rest of monolayer WSe_2 in the vicinity, forming n-doped monolayer WSe_2 and hole-dominant WO_3. It is worth noting that the GSB peaks for C-exciton and A-exciton states of monolayer WSe_2 are always clearly observed under the Mott density condition, and the initial C-exciton signal in IFsLI case 2 even increases again, implying a higher initial carrier population in this band-nesting state. Exciton-density-dependent initial amplitudes for the four GSB peaks are summarized in Fig. S4 (ESI†). These results indicate that the electronic states observed in TA spectra at a given delay time could be used to *in situ* characterize the IFsLI-related modification degree for monolayer WSe_2 right after the exposure of each laser shot and quantitatively find the lowest modification threshold, which is related to the Mott density of TMDCs.

Fig. 3 shows theoretically calculated band structures of perfect monolayer WSe_2, monolayer WSe_2 with V_{Se} (one Se vacancy), and monolayer WSe_2 with O_{Se} (one Se is replaced by one O). For the systems with a hexagonal shape, the *K* point in the Brillouin zone of the unit cell will be folded into the Gamma point in the Brillouin zone of the $6 \times 6 \times 1$ supercell.[49] It leads to the VBM of perfect WSe_2 at the Gamma point in calculated band structures. The defect states of V_{Se} are removed when the Se vacancy is occupied by O, and the resulting bandgap is still larger than that of pristine monolayer WSe_2.[50] This is consistent with our TA experimental results, which facilitate the formation of n-doped monolayer WSe_2 in the IFsLI-treatment. The formation energies of V_{Se} and O_{Se} in monolayer WSe_2 are listed in Table S3 (ESI†). Compared to monolayer WSe_2 with V_{Se}, monolayer WSe_2 with O_{Se} has much lower formation energy, which is even negative for the O atom from the O_2 reservoir under ambient conditions. It reveals that to create a Se vacancy needs a lot of extra energies, like under electron/neutron beam irradiation or intense laser irradiation, but once the Se vacancy occurs, it is very easily passivated by the O atom (it works in the case where the chemical potential of O atom is referred to its reservoir O_2 or WO_3).

The TA experiments on monolayer WSe_2 covered by graphene further support our understanding. Fig. S5 (ESI†) shows the steady-state absorption spectra of graphene and monolayer WSe_2 covered by graphene. It is notable that under the same low pump conditions (*i.e.*, initial exciton density of 9.20×10^{11} cm^{-2}), the amplitude of GSB signals for each exciton state is comparable for monolayer WSe_2 with/without graphene. It suggests the influence of graphene on the estimated initial exciton densities is minor and can be negligible under our experimental conditions. It is found that when the monolayer WSe_2 is covered by graphene, it inhibits the participation of O atoms for the oxidizing of Se vacancies since graphene has a high-energy barrier for the surface oxidation reaction and its atomically thin thickness is also enough to

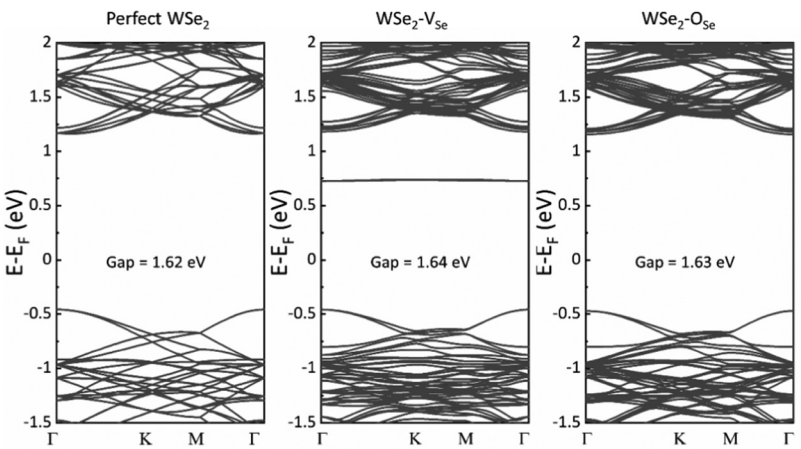

Fig. 3 Band structures of (left) perfect WSe_2, (middle) WSe_2 with V_{Se} (one Se vacancy), and (right) WSe_2 with one O_{Se} (one Se is replaced by one O). The Fermi level is at 0 eV.

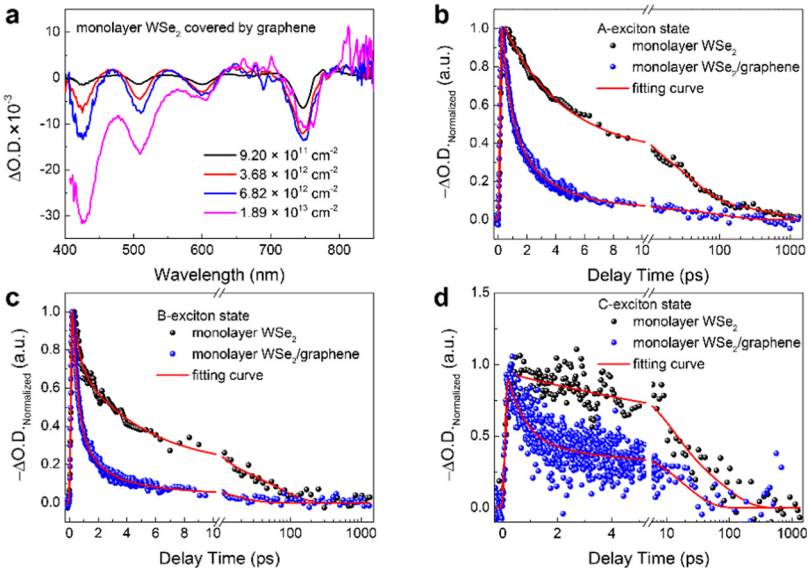

Fig. 4 (a) Initial TA spectra of graphene-covered monolayer WSe_2 films probed at 0.25 ps under 400 nm at different initial exciton densities from 9.20×10^{11} cm^{-2} to 1.89×10^{13} cm^{-2}. The normalized dynamics of (b) A-, (c) B-exciton and (d) C-exciton states of monolayer WSe_2 with and without graphene under 400 nm excitation at an initial exciton density of 9.20×10^{11} cm^{-2}. The red solid lines are the multiple-exponential fitting results.

physically separate the existed Se vacancies in monolayer WSe_2 from O atoms under ambient conditions.[51] As a result, there is no observation of oxygen-related transient species in the initial time of TA data (Fig. 4a), and the exciton population is preferentially dominated by the A′- and C-exciton states under the Mott density condition (in the meantime, the amplitude of GSB signals for A- and B-exciton states is not greatly decreased), probably due to the band nesting effect and the band renormalization under those ultrahigh initial exciton densities.[26,35,52] This also indicates that IFsLI treatments under our experimental conditions are not strong enough to directly remove Se atoms in monolayer WSe_2 forming Se vacancies. It in turn means the IFsLI-related modification mechanism in monolayer WSe_2 is not the case of directly creating new Se vacancies first by IFsLI treatments; instead, it is an IFsLI-assisted excited-state photochemical reaction: when IFsLI increases the initial exciton density of monolayer WSe_2 to the Mott density condition, monolayer WSe_2 prefers to resist the Mott transition by the band renormalization and/or the photochemical reaction with O atoms under ambient conditions. For the latter, an IFsLI-related modification occurs in monolayer WSe_2, where the modification threshold is around the Mott density. In addition, there is an efficient charge transfer from the band-edge states and C-exciton state of monolayer WSe_2 to graphene in graphene-covered monolayer WSe_2, which is estimated to be 89%, 86% and 79% for A-, B- and C-exciton states, respectively, in comparison with that in monolayer WSe_2 only (Fig. 4b–d). Detailed fitting data are presented in Table S4 (ESI†). These control experiments indicate that graphene plays a dual role in graphene-covered monolayer TMDCs, which is the protection of samples from oxygen doping and initial carrier extraction from monolayer TMDCs.

Conclusions

In conclusion, we have presented key stages of electronic state evolution for IFsLI-treated monolayer WSe_2 around the modification threshold by broadband TA experiments. Steady-state absorption/PL/Raman/XPS measurements and first-principles calculations confirm the existence of IFsLI-related oxidization for monolayer WSe_2. Different from the direct removal of atoms in samples, control experiments on monolayer WSe_2 covered by graphene further demonstrate that it is an IFsLI-assisted photochemical reaction and reveal an efficient initial carrier extraction for the band-edge exciton states in monolayer WSe_2. Our findings provide an electronic state criterion to *in situ* monitor the degrees of modification in monolayer TMDCs during the femtosecond laser modification. It also indicates a simple laser fabrication approach for lateral monolayer heterojunctions, due to the IFsLI-assisted oxidization reaction for monolayer TMDCs.

Author contributions

The manuscript was written through contributions of all authors. All authors have given approval for the final version of the manuscript.

Conflicts of interest

There are no conflicts to declare.

Acknowledgements

The authors would like to acknowledge the Natural Science Foundation of China (NSFC) under Grant No. #62175088,

#61927814, #21773087, #21603083, and #21903035, and the China Postdoctoral Science Foundation under Grant No. 2016M590259 for support.

References

1 F. N. Xia, H. Wang, D. Xiao, M. Dubey and A. Ramasubramaniam, *Nat. Photonics*, 2014, **8**, 899–907.
2 S. F. Wu, S. Buckley, J. R. Schaibley, L. F. Feng, J. Q. Yan, D. G. Mandrus, F. Hatami, W. Yao, J. Vuckovic, A. Majumdar and X. D. Xu, *Nature*, 2015, **520**, 69–72.
3 P. F. Qi, Y. Luo, B. B. Shi, W. Li, D. L. Liu, L. H. Zheng, Z. X. Liu, Y. L. Hou and Z. Y. Fang, *eLight*, 2021, **1**, 6.
4 H. Lin, B. C. P. Sturmberg, K. T. Lin, Y. Y. Yang, X. R. Zheng, T. K. Chong, C. M. de Sterke and B. H. Jia, *Nat. Photonics*, 2019, **13**, 270–276.
5 L. Jia, W. Zheng and F. Huang, *PhotoniX*, 2020, **1**, 22.
6 R. Kumar, N. Goel, M. Hojamberdiev and M. Kumar, *Sens. Actuators, A*, 2020, **303**, 111875.
7 A. Kuc, T. Heine and A. Kis, *MRS Bull.*, 2015, **40**, 577–584.
8 Z. B. Li and S. L. Wong, *Mater. Sci. Eng., C*, 2017, **70**, 1095–1106.
9 D. Wang, X. B. Li, D. Han, W. Q. Tian and H. B. Sun, *Nano Today*, 2017, **16**, 30–45.
10 T. D. Ngo, M. S. Choi, M. Lee, F. Ali, Y. Hassan, N. Ali, S. Liu, C. Lee, J. Hone and W. J. Yoo, *Adv. Sci.*, 2022, **9**, 2202465.
11 Z. N. Guo, Y. H. Zeng, F. X. Meng, H. Z. Qu, S. L. Zhang, S. P. Hu, S. D. Fan, H. B. Zeng, R. Cao, P. N. Prasad, D. Y. Fan and H. Zhang, *eLight*, 2022, **2**, 9.
12 S. Yang, G. Lee, J. Kim, S. Yang, C. H. Lee and J. Kim, *J. Mater. Chem. C*, 2020, **8**, 8393–8398.
13 J. Chen, Q. Y. Wang, Y. C. Sheng, G. Q. Cao, P. Yang, Y. B. Shan, F. Y. Liao, Z. Muhammad, W. Z. Bao, L. G. Hu, R. Liu, C. X. Cong and Z. J. Qiu, *ACS Appl. Mater. Interfaces*, 2019, **11**, 43330–43336.
14 H. Lin, Z. Q. Xu, G. Y. Cao, Y. P. Zhang, J. D. Zhou, Z. Y. Wang, Z. C. Wan, Z. Liu, K. P. Loh, C. W. Qiu, Q. L. Bao and B. H. Jia, *Light: Sci. Appl.*, 2020, **9**, 137.
15 C. Zhu, X. X. Zhao, X. W. Wang, J. Q. Chen, P. Yu, S. Liu, J. D. Zhou, Q. D. Fu, Q. S. Zeng, Y. M. He, J. H. Edgar, S. J. Pennycook, F. C. Liu and Z. Liu, *Adv. Funct. Mater.*, 2021, **31**, 2009549.
16 X. W. Wang, B. L. Wang, Q. H. Zhang, Y. F. Sun, E. Z. Wang, H. Luo, Y. H. Wu, L. Gu, H. L. Li and K. Liu, *Adv. Mater.*, 2021, **33**, 2102435.
17 R. J. Stöhr, R. Kolesov, K. W. Xia and J. Wrachtrup, *ACS Nano*, 2011, **5**, 5141–5150.
18 Z. Z. Li, L. Wang, H. Fan, Y. H. Yu, H. B. Sun, S. Juodkazis and Q. D. Chen, *Light: Sci. Appl.*, 2020, **9**, 41.
19 B. R. Gao, H. Y. Wang, Y. W. Hao, L. M. Fu, H. H. Fang, Y. Jiang, L. Wang, Q. D. Chen, H. Xia, L. Y. Pan, Y. G. Ma and H. B. Sun, *J. Phys. Chem. B*, 2010, **114**, 128.
20 M. M. Wang, D. W. Li, K. Liu, Q. T. Guo, S. M. Wang and X. Li, *ACS Nano*, 2020, **14**, 11169–11177.
21 M. Currie, J. D. Caldwell, F. J. Bezares, J. Robinson, T. Anderson, H. D. Chun and M. Tadjer, *Appl. Phys. Lett.*, 2011, **99**, 211909.
22 D. Wang, D. Han, X. B. Li, S. Y. Xie, N. K. Chen, W. Q. Tian, D. West, H. B. Sun and S. B. Zhang, *Phys. Rev. Lett.*, 2015, **114**, 196801.
23 X. B. Li, X. Q. Liu, X. Liu, D. Han, Z. Zhang, X. D. Han, H. B. Sun and S.-B. Zhang, *Phys. Rev. Lett.*, 2011, **107**, 015501.
24 H. Zheng, X. B. Li, N. K. Chen, S. Y. Xie, W. Q. Tian, Y. Chen, H. Xia, S. B. Zhang and H. B. Sun, *Phys. Rev. B: Condens. Matter Mater. Phys.*, 2015, **92**, 115307.
25 H. Wang, H. Y. Wang, Q. D. Chen, H. L. Xu, H. B. Sun, F. C. Huang, W. Raja, A. Toma and R. P. Zaccaria, *Laser Photonics Rev.*, 2018, **12**, 1700176.
26 L. Wang, Z. Wang, H. Y. Wang, G. Grinblat, Y. L. Huang, D. Wang, X. H. Ye, X. B. Li, Q. L. Bao, A. S. Wee, S. A. Maier, Q. D. Chen, M. L. Zhong, C. W. Qiu and H. B. Sun, *Nat. Commun.*, 2017, **8**, 13906.
27 R. Ding, X. P. Wang, J. Feng, X. B. Li, F. X. Dong, W. Q. Tian, J. R. Du, H. H. Fang, H. Y. Wang, T. Yamao, S. Hotta and H. B. Sun, *Adv. Mater.*, 2018, **30**, 1801078.
28 W. Kohn and L. J. Sham, *Phys. Rev.*, 1965, **140**, A1133.
29 P. Hohenberg and W. Kohn, *Phys. Rev.*, 1964, **136**, B864.
30 X. B. Li, N. K. Chen, X. P. Wang and H. B. Sun, *Adv. Funct. Mater.*, 2018, **28**, 1803380.
31 E. Goi, Q. Zhang, X. Chen, H. Luan and M. Gu, *PhotoniX*, 2020, **1**, 3.
32 G. Kresse and J. Furthmüller, *Comput. Mater. Sci.*, 1996, **6**, 15.
33 G. Kresse and J. Furthmüller, *Phys. Rev. B: Condens. Matter Mater. Phys.*, 1996, **54**, 11169.
34 J. P. Perdew, K. Burke and M. Ernzerhof, *Phys. Rev. Lett.*, 1996, **77**, 3865.
35 X. Chen, Z. Wang, L. Wang, H. Y. Wang, Y. Y. Yue, H. Wang, X. P. Wang, A. T. S. Wee, C. W. Qiu and H. B. Sun, *Nanoscale*, 2018, **10**, 9346.
36 X. Chen, L. Wang, H. Y. Wang, X. P. Wang, Y. Luo and H. B. Sun, *J. Phys. D: Appl. Phys.*, 2021, **54**, 354002.
37 S. W. Zheng, H. Y. Wang, L. Wang, Y. Luo, B. R. Gao and H. B. Sun, *Nanoscale*, 2021, **13**, 14081.
38 X. Chen, S. W. Zheng, X. P. Wang and H. Y. Wang, *Phys. Chem. Chem. Phys.*, 2022, **24**, 16538–16544.
39 H. G. Ji, P. Solís-Fernández, D. Yoshimura, M. Maruyama, T. Endo, Y. Miyata, S. Okada and H. Ago, *Adv. Mater.*, 2019, **31**, 1903613.
40 J. H. Jung and W. Choi, *Mater. Lett.*, 2021, **295**, 129865.
41 S. M. Eichfeld, L. Hossain, Y. C. Lin, A. F. Piasecki, B. Kupp, A. G. Birdwell, R. A. Burke, N. Lu, X. Peng, J. Li, A. Azcatl, S. McDonnell, R. M. Wallace, M. J. Kim, T. S. Mayer, J. M. Redwing and J. A. Robinson, *ACS Nano*, 2015, **9**, 2080–2087.
42 X. T. Zhang, T. H. Choudhury, M. Chubarov, Y. Xiang, B. Jariwala, F. Zhang, N. Alem, G. C. Wang, J. A. Robinson and J. M. Redwing, *Nano Lett.*, 2018, **18**, 1049–1056.
43 T. J. Zhang and J. Wang, *ACS Photonics*, 2021, **8**, 2770–2780.
44 D. Li, R. T. Chen, S. Y. Wang, X. W. Zhang, Y. Zhang, J. X. Liu, H. Yin, F. T. Fan, J. Y. Shi and C. Li, *J. Phys. Chem. Lett.*, 2020, **11**, 412–418.
45 F. M. Pesci, A. J. Cowan, B. D. Alexander, J. R. Durrant and D. R. Klug, *J. Phys. Chem. Lett.*, 2011, **2**, 1900–1903.

46 X. P. Zhai, L. F. Gao, H. Zhang, Y. Peng, X. D. Zhang, Q. Wang and H. L. Zhang, *ACS Appl. Nano Mater.*, 2022, **5**, 1169–1177.
47 L. J. Zhang, S. Li, B. K. Liu and T. F. Xie, *ACS Catal.*, 2014, **4**, 3724–3729.
48 H. J. Li, Y. Y. Gao, Y. Zhou, F. T. Fan, Q. T. Han, Q. F. Xu, X. Y. Wang, M. Xiao, C. Li and Z. G. Zou, *Nano Lett.*, 2016, **16**, 5547–5552.
49 F. Aikebaier, A. Pertsova and C. M. Canali, *Phys. Rev. B: Condens. Matter Mater. Phys.*, 2015, **92**, 155420.
50 Q. L. Cui, Z. Y. Luo, Q. R. Cui, W. Zhu, H. W. Shou, C. Q. Wu, Z. F. Liu, Y. X. Lin, P. J. Zhang, S. Q. Wei, H. X. Yang, S. M. Chen, A. L. Pan and L. Song, *Adv. Funct. Mater.*, 2021, **31**, 2105339.
51 M. Topsakal, H. Sahin and S. Ciraci, *Phys. Rev. B: Condens. Matter Mater. Phys.*, 2012, **85**, 155445.
52 Y. Y. Yue, Z. Wang, L. Wang, H. Y. Wang, Y. Chen, D. Wang, Q. D. Chen, B. R. Gao, A. T. S. Wee, C. W. Qiu and H. B. Sun, *Nanotechnology*, 2021, **32**, 135208.